nature photonics

SUPPLEMENTARY INFORMATION

https://doi.org/10.1038/s41566-020-0668-z

In the format provided by the authors and unedited.

Fast spin-flip enables efficient and stable organic electroluminescence from charge-transfer states

Lin-Song Cui[1,8]✉, Alexander J. Gillett[1,8], Shou-Feng Zhang[2,3,8], Hao Ye[4], Yuan Liu[5], Xian-Kai Chen[3]✉, Ze-Sen Lin[4], Emrys W. Evans[1], William K. Myers[6], Tanya K. Ronson[7], Hajime Nakanotani[4], Sebastian Reineke[5], Jean-Luc Bredas[3], Chihaya Adachi[4]✉ and Richard H. Friend[1]✉

[1]Cavendish Laboratory, University of Cambridge, Cambridge, UK. [2]Department of Electronic Engineering, Guangxi University of Science and Technology, Liuzhou, China. [3]School of Chemistry and Biochemistry, Center for Organic Photonics and Electronics, Georgia Institute of Technology, Atlanta, GA, USA. [4]Center for Organic Photonics and Electronics Research (OPERA), Kyushu University, Fukuoka, Japan. [5]Dresden Integrated Center for Applied Physics and Photonic Materials (IAPP), Technische Universität Dresden, Dresden, Germany. [6]Centre for Advanced Electron Spin Resonance (CAESR), University of Oxford, Oxford, UK. [7]Department of Chemistry, University of Cambridge, Cambridge, UK. [8]These authors contributed equally: Lin-Song Cui, Alexander J. Gillett, Shou-Feng Zhang. ✉e-mail: lc724@cam.ac.uk; chenxiankai@email.arizona.edu; adachi@cstf.kyushu-u.ac.jp; rhf10@cam.ac.uk

Fast Spin-Flip Enables Efficient and Stable Organic Electroluminescence from Charge-Transfer States

Lin-Song Cui[1,8,*], Alexander J. Gillett[1,8], Shou-Feng Zhang[2,3,8], Hao Ye[4], Yuan Liu[5], Xian-Kai Chen[3,*], Ze-Sen Lin[4], Emrys W. Evans[1], William K. Myers[6], Tanya K. Ronson[7], Hajime Nakanotani[4], Sebastian Reineke[5], Jean-Luc Bredas[3], Chihaya Adachi [4,*], Richard H. Friend[1,*]

[1]Cavendish Laboratory, University of Cambridge, JJ Thomson Avenue, Cambridge, CB3 0HE, United Kingdom.

[2]Department of Electronic Engineering, Guangxi University of Science and Technology, Liuzhou 545006, China

[3]School of Chemistry and Biochemistry, Center for Organic Photonics and Electronics, Georgia Institute of Technology, Atlanta, GA, 30332-0400, USA

[4]Center for Organic Photonics and Electronics Research (OPERA), Kyushu University, 744 Motooka, Nishi, Fukuoka 819-0395, Japan.

[5]Dresden Integrated Center for Applied Physics and Photonic Materials (IAPP), Technische Universität Dresden, Dresden, 01069, Germany.

[6]Centre for Advanced Electron Spin Resonance (CAESR), University of Oxford, South Parks Road, Oxford, OX1 3QR, UK.

[7]Department of Chemistry, University of Cambridge, Lensfield Road, Cambridge, CB1EW, United Kingdom.

[8]These authors contributed equally to this work: Lin-Song Cui, Alexander J. Gillett, Shou-Feng Zhang

[*]Corresponding author. Lin-Song Cui: E-mail: lc724@cam.ac.uk; Xian-Kai Chen: E-mail: chenxiankai@email.arizona.edu; Chihaya Adachi: E-mail: adachi@cstf.kyushu-u.ac.jp; Richard H. Friend: E-mail: rhf10@cam.ac.uk.

Contents

S1. Materials synthesis and characterization

Materials and methods. All reagents were used as received from commercial sources and were used without further purification. 2-chloro-4,6-diphenyl-1,3,5-triazine, pentafluorophenylboronic acid, palladium(II) acetate and cesium carbonate were purchased from TCI. Chromatographic separations were carried out using silica gel (200–300 nm). The materials were further purified by temperature-gradient vacuum sublimation to obtain high-purity materials for the device evaluations. ^{1}H nuclear magnetic resonance (NMR) and ^{13}C NMR spectra were obtained in $CDCl_2$ with a Bruker Biospin Avance-III 500 NMR spectrometer at ambient temperature. BRUKER ultrafleXtreme MALDI-TOF/TOF was employed to measure Matrix-Assisted Laser Desorption/Ionization Time of Flight Mass Spectrometry (MALDI-TOF-MS). Elemental analyses (C, H and N) were carried out with a Yanaco MT-5 elemental analyzer.

Synthesis. 5Cz-TRZ was synthesized through a two-step process from pentafluorobenzeneboronic acid. The stepwise synthetic methods are shown in Scheme S1 and the general process is given below.

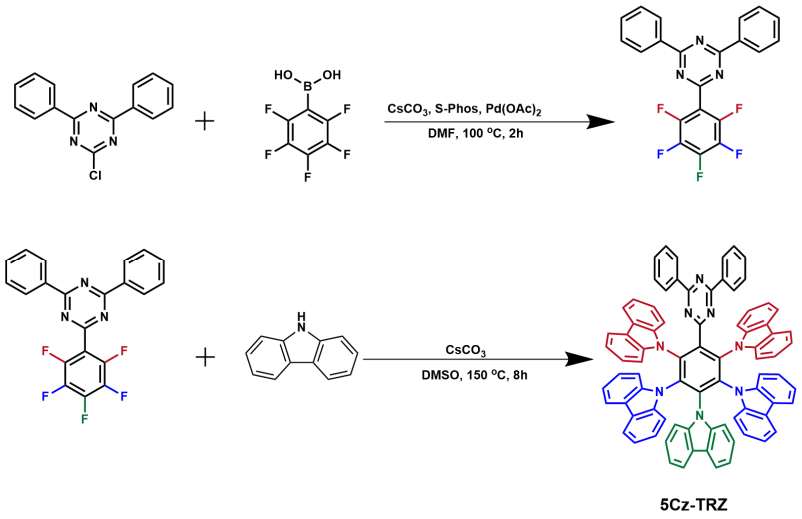

Scheme S1. Synthesis of 5Cz-TRZ

Synthesis of 2-(perfluorophenyl)-4,6-diphenyl-1,3,5-triazine. A mixture of 2-chloro-4,6-diphenyl-1,3,5-triazine (1.34 g, 5.01 mmol), pentafluorobenzeneboronic acid (2.12 g, 10.02 mmol), palladium(II) acetate (0.06 g, 0.25 mmol), 2-dicyclohexylphosphino-2',6'-dimethoxybiphenyl (0.82 g, 2.02 mmol) and cesium carbonate (6.52 g, 20.02 mmol) in 30 mL of DMF in a 100 mL round bottom was refluxed for 2 hours under argon. The mixture was extracted with chloroform. The combined organic extracts were dried over Na_2SO_4 and concentrated by rotary evaporation. The crude product was purified by column chromatography on silica gel using 1: 4 ethyl acetate/petroleum as eluent to afford a white solid (1.04 g, 52 % yield). M. P. 223.3 °C. ^{1}H NMR (500 MHz,

CD_2Cl_2) δ (ppm): 8.60 (d, *J* = 8.0 Hz, 4H), 7.57 (t, *J* = 7.0 Hz, 2H), 7.50 (t, *J* = 7.5 Hz, 4H).^{13}C NMR (125 MHz, CD_2Cl_2) δ (ppm): 172.17 (s), 166.36 (s), 146.95 (m), 144.41 (m), 141.27 (m), 139.16 (m), 136.64 (m), 133.24 (s), 129.19 (s), 128.85 (s), 113.49(m). ^{19}F NMR (471 MHz, CD_2Cl_2) δ (ppm): −140.97 (m, 2F), −151.02 (m, 1F), −161.22 (m, 2F). MS *m/z*: 399.26 $[M]^+$. Anal. calcd for $C_{21}H_{10}F_5N_3$ (%): C 63.16, H 2.52, N 10.52; found: C 63.15, H 2.54, N 10.54.

Synthesis of 9,9',9'',9''',9''''-((1s,2r,3r,4s,5s)-6-(4,6-diphenyl-1,3,5-triazin-2-yl)benzene-1,2,3,4,5-pentayl)pentakis(9H-carbazole) (5Cz-TRZ). Under argon atmosphere carbazole (1.67 g, 10.00 mmol) was added to a two necked round bottom flask equipped with a reflux condenser. Addition of cesium carbonate (13.03 g, 40.00 mmol) followed by DMF (100 mL) resulted in a suspension, which was stirred for 30 min at room temperature. Afterwards, 2-(perfluorophenyl)-4,6-diphenyl-1,3,5-triazine (0.80 g, 2.00 mmol) was poured in all in once and reaction mixture was stirred at 155°C for 12 hours. The black mixture was diluted with water and crude product was extracted with chloroform (3 × 30 mL). Organic phases were dried over Na_2SO_4 and solvent was removed. 5Cz-TRZ (1.47 g, 0.13 mmol, 65%) was isolated as white solid after purification by column chromatography on silica gel using 1: 4 dichloromethane/ petroleum as eluent. M. P. 473.7 ^{o}C. ^{1}H NMR (500 MHz, CD_2Cl_2) δ (ppm): δ 7.53 (d, *J* = 7.5 Hz, 4H), 7.50 – 7.39 (m, 14H), 7.38 – 7.33 (m, 4H), 7.17 (d, *J* = 8.0 Hz, 4H), 7.07(t, *J* = 7.5 Hz, 4H), 7.04 – 6.94(m, 8H), 6.89 – 6.76 (m, 10H), 6.70 (t, *J* = 7.5 Hz, 2H). ^{13}C NMR (125 MHz, CD_2Cl_2) δ (ppm): 140.30, 138.74, 138.19, 137.56, 134.34, 132.13, 128.26, 128.01, 125.02, 124.46, 123.52, 123.33, 120.11, 120.07, 119.81, 119.34, 119.20, 110.95, 110.88, 110.34. MS *m/z*: 1134.32 $[M]^+$. Anal. calcd for $C_{81}H_{50}N_8$ (%): C 85.69, H 4.44, N 9.87; found: C 85.70, H 4.42, N 9.88.

S2. Computational data

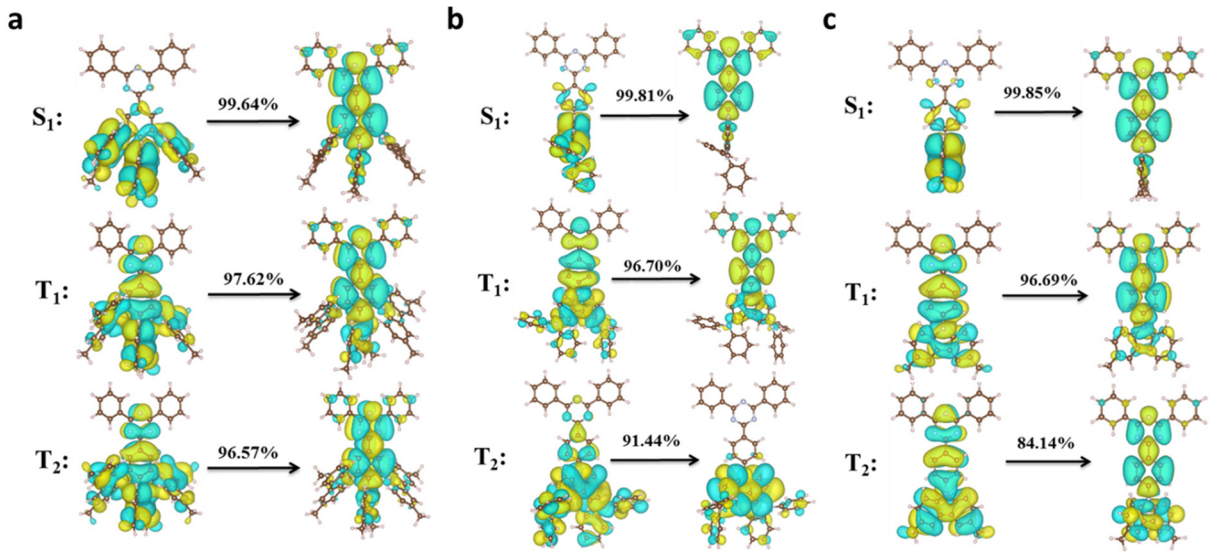

Fig. S1. Natural Transition Orbitals (NTO) describing the excitation characters of the S_1, T_1, and T_2 states in TmCz-TRZ (a), DACT-II (b), and mCz-TRZ (c). The weights of the hole–electron contributions to the excitations are included.

Table S1. Energy gaps ($\Delta E_{S1\text{-}T1}/\Delta E_{S1\text{-}T2}$) between the adiabatic excitation energies of the S_1 and T_1/T_2 states and spin-orbit couplings ($SOC_{S1\text{-}T1}/SOC_{S1\text{-}T2}$), as calculated at the TDA tuned-ωB97XD/6-31G(d,p) level of theory; transition rates ($k_{T1\rightarrow S1}/k_{T2\rightarrow S1}$) from T_1/T_2 to S_1 evaluated via the Marcus electron-transfer rate equation.

	$\Delta E_{S1\text{-}T1}$ / eV	$\Delta E_{S1\text{-}T2}$ / eV	$SOC_{S1\text{-}T1}$ / cm^{-1}	$SOC_{S1\text{-}T2}$ / cm^{-1}	$k_{T1\rightarrow S1}$ / s^{-1}	$k_{T2\rightarrow S1}$ / s^{-1}
5Cz-TRZ	0.02	-0.23	0.4	1.3	4.1×10^6	1.4×10^9
TmCz-TRZ	0.24	-0.06	0.4	0.6	2.5×10^5	1.3×10^7
DACT-II	0.28	-0.27	0.3	0.3	5.6×10^4	3.1×10^7
mCz-TRZ	0.64	-0.08	0.1	0.2	3.7×10^2	2.3×10^4

S3. Thermal properties

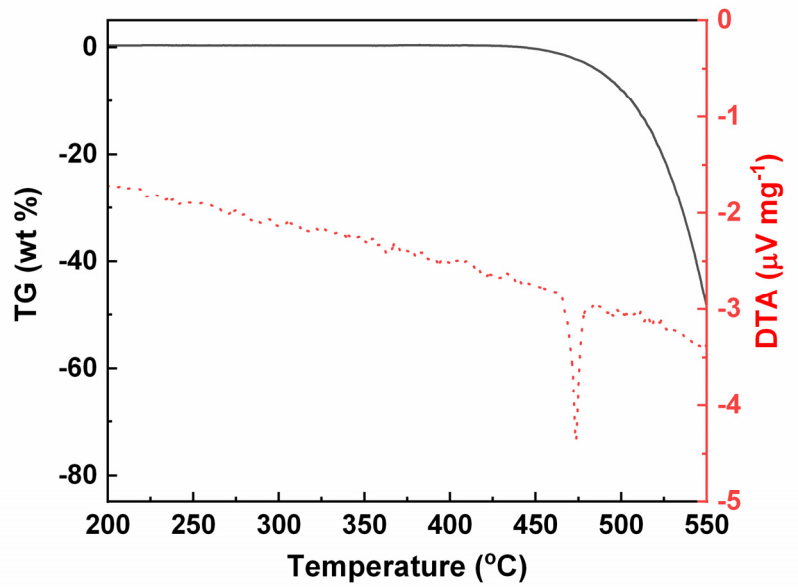

Fig. S2. Thermal stability properties (TG-DTA) of 5Cz-TRZ.

S4. Photophysical properties

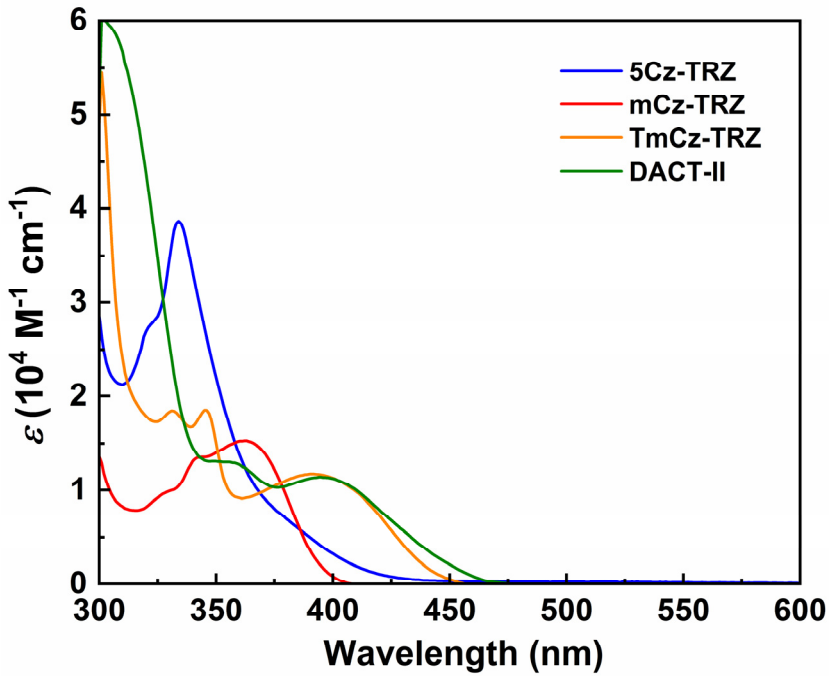

Fig. S3. UV-Vis absorption spectra of 5Cz-TRZ, mCz-TRZ, TmCz-TRZ and DACT-II in toluene solution.

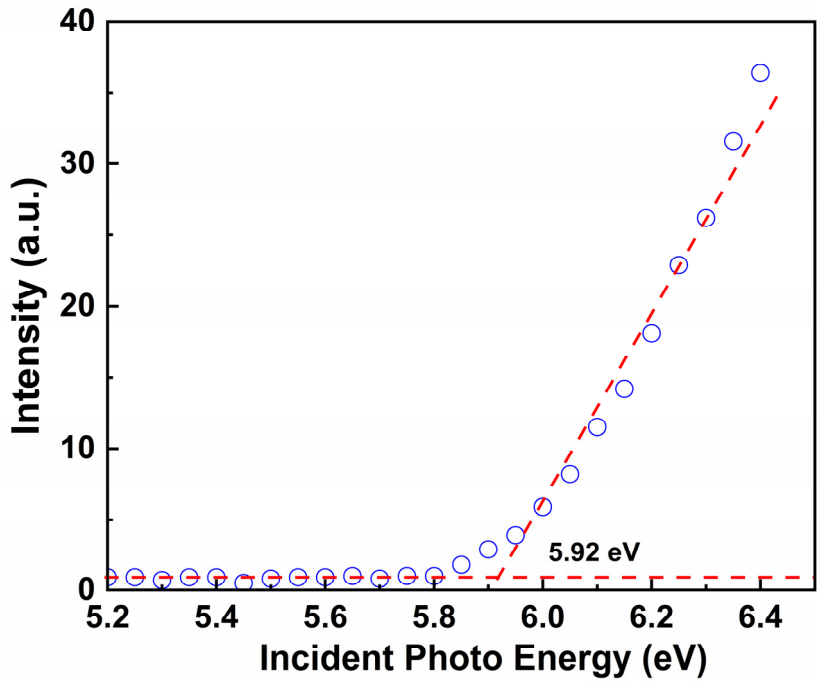

Fig. S4. Photoelectron spectral measurement of 5Cz-TRZ neat film under nitrogen atmosphere.

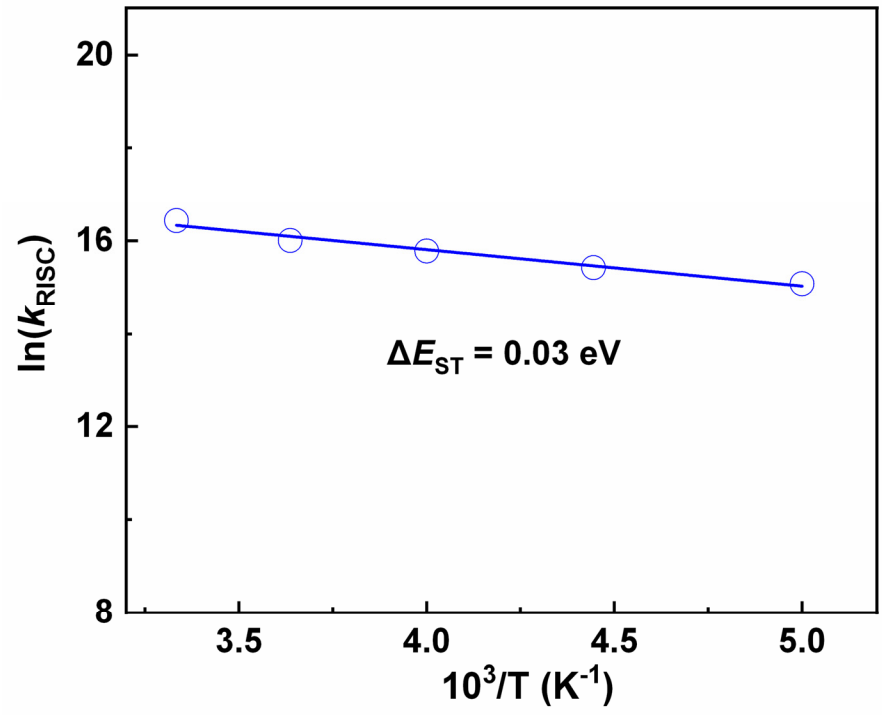

Fig. S5. Arrhenius plot of the RISC rate from the triplet state to the singlet state of 5Cz-TRZ in doped film.

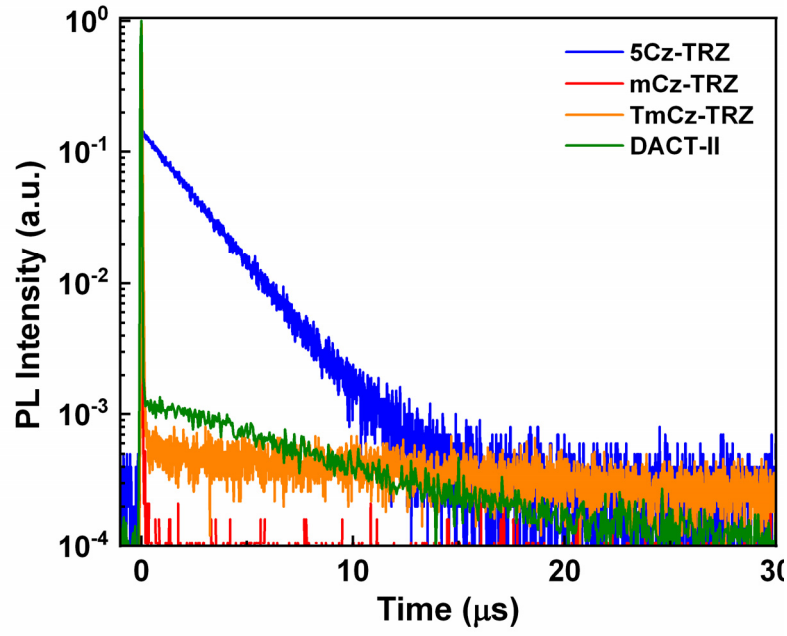

Fig. S6. Transient PL spectra (300 K) of 5Cz-TRZ, mCz-TRZ, TmCz-TRZ and DACT-II in oxygen-free toluene.

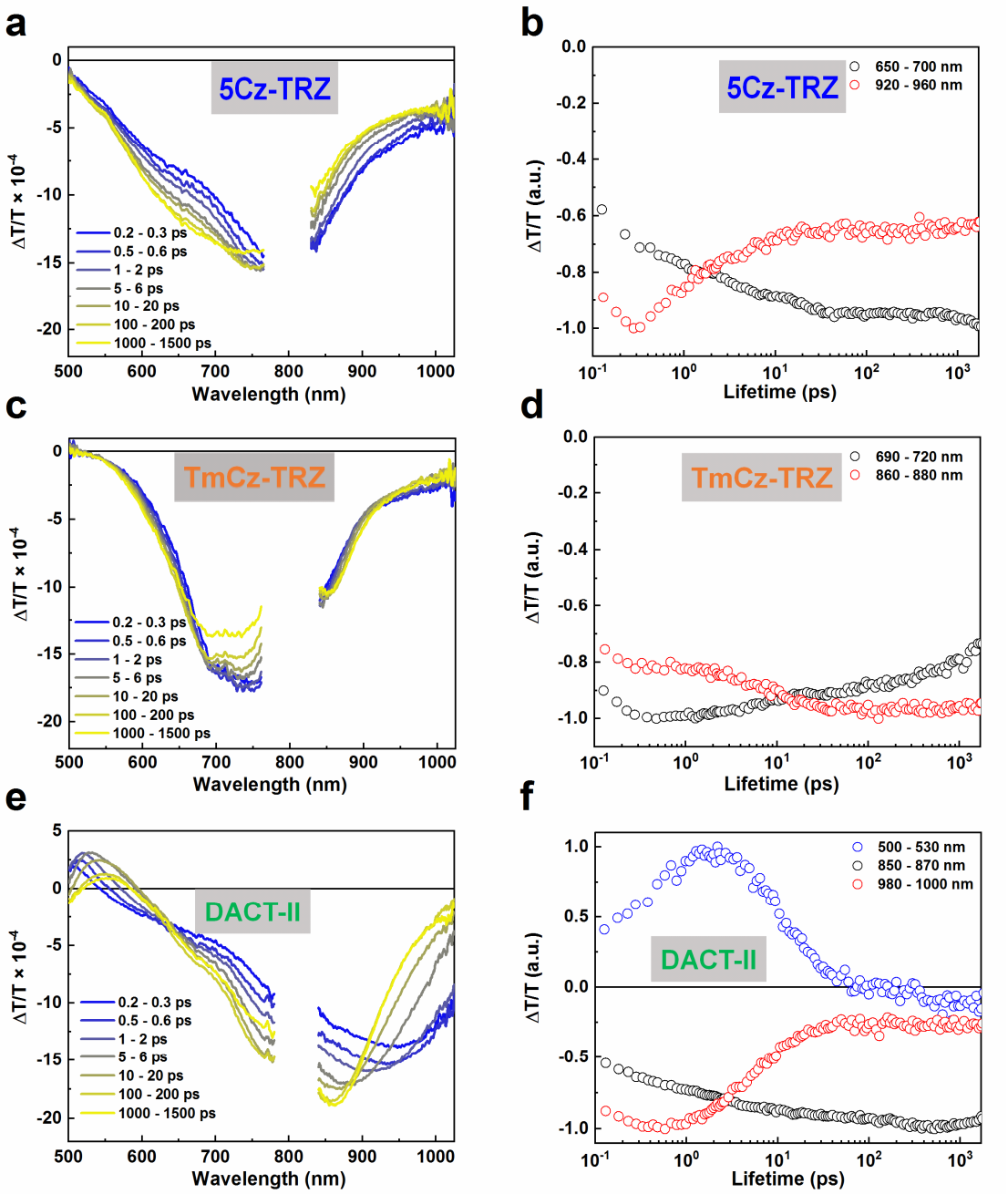

Fig. S7. Transient absorption spectra and normalized kinetics on picosecond timescales in oxygen-free toluene solutions. **a, c, e,** Transient absorption spectra of 5Cz-TRZ (a), TmCz-TRZ (c) and DACT-II (e). **b, d, f,** Normalized kinetics of 5Cz-TRZ (b), TmCz-TRZ (d) and DACT-II (f).

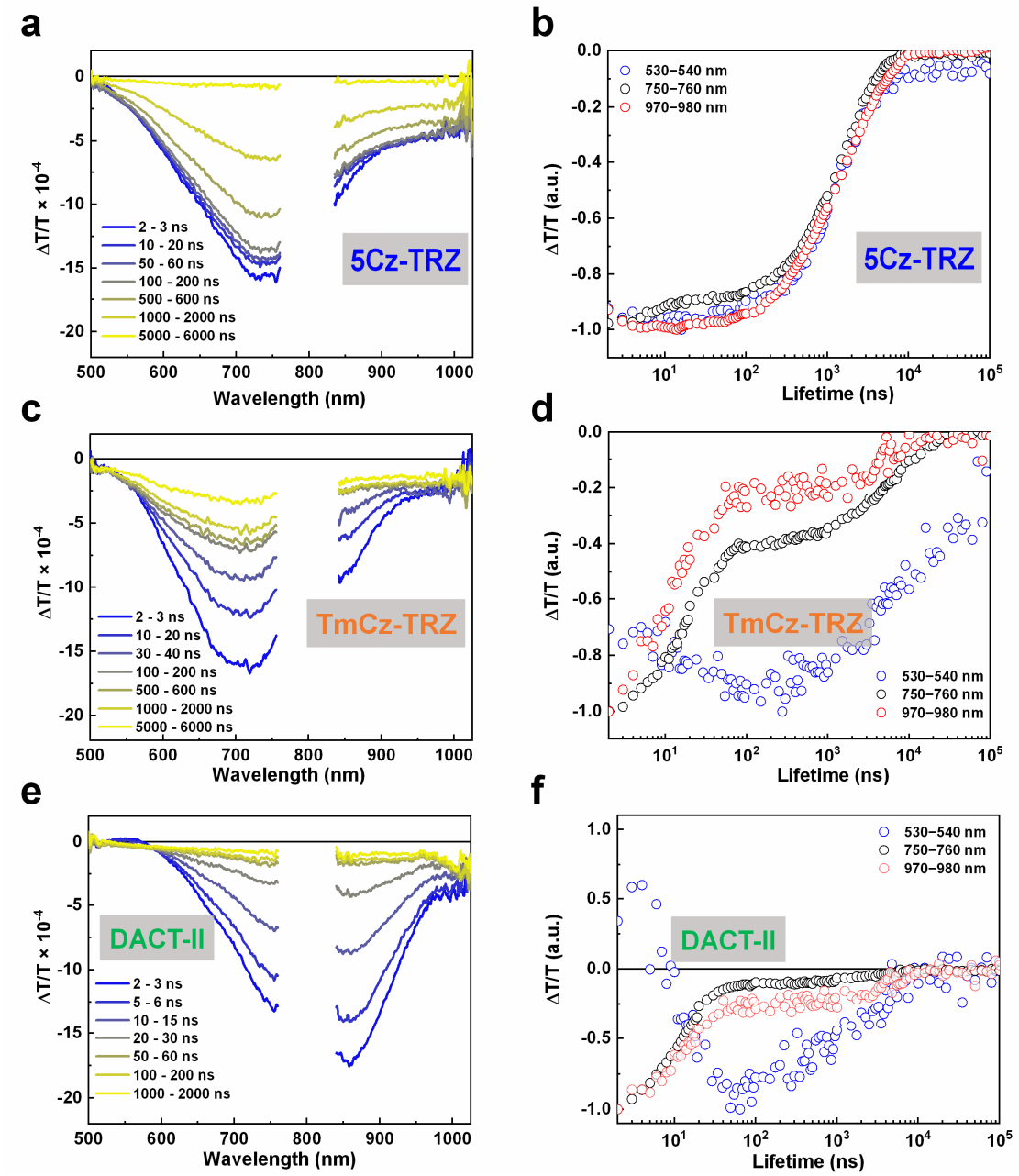

Fig. S8. Transient absorption spectra and normalized kinetics on nanosecond timescales in oxygen-free toluene solutions. **a, c, e,** Transient absorption spectra of 5Cz-TRZ (a), TmCz-TRZ (c) and DACT-II (e), respectively. **b, d, f,** Normalized kinetics of 5Cz-TRZ (b), TmCz-TRZ (d) and DACT-II (f), respectively.

In the picosecond TA, excited at 400 nm, all molecules exhibit similar behaviour. A rapid spectral shift in the photo-induced absorption (PIA) features occurs within the first 10 ps. This is assigned to molecular relaxation processes, likely involving solvent re-orientation given the relatively long timescales involved. Indeed, in DACT-II, the red-shifting of the stimulated emission (SE) band around 500 – 600 nm can be observed over the same timescales as the PIA shift, confirming that these processes involve a relaxation of singlet excited state. After

relaxation of the singlet state has occurred, there are very few spectral shifts over the remainder of the picosecond TA measurements.

Turning next to the nanosecond TA measurements, excited at 355 nm, we initially observe similar PIA features to the relaxed singlet PIAs in the picosecond TA, as expected. For 5Cz-TRZ, there is a PIA band peaked at around 750 nm. In TmCz-TRZ, there is a PIA peaked at 710 nm. Finally, in DACT-II, there is a PIA centred at around 850 nm. In 5Cz-TRZ, there is very little loss of PIA intensity within the first 200 ns, indicating the vast majority of excited states undergo ISC into the triplet manifold, instead of decay directly from the singlet. In contrast, there is a significant decrease in PIA intensity for TmCz-TRZ and DACT-II within 200 ns, suggesting a significant proportion of singlet states either emit or decay non-radiatively before they are able to undergo ISC. This picture is consistent with the substantially higher SOC in 5Cz-TRZ, allowing ISC to out-compete radiative and non-radiative singlet decay in this material. All molecules show distinct biphasic decays, in-line with the prompt-delayed emission behaviour observed in TADF materials. The delayed-component lifetime of 5Cz-TRZ is the shortest, consistent with the picture seen in both the transient PL and EL decay measurements, suggesting that this material also possesses the most rapid RISC, again aided by the largest SOC value in the material series.

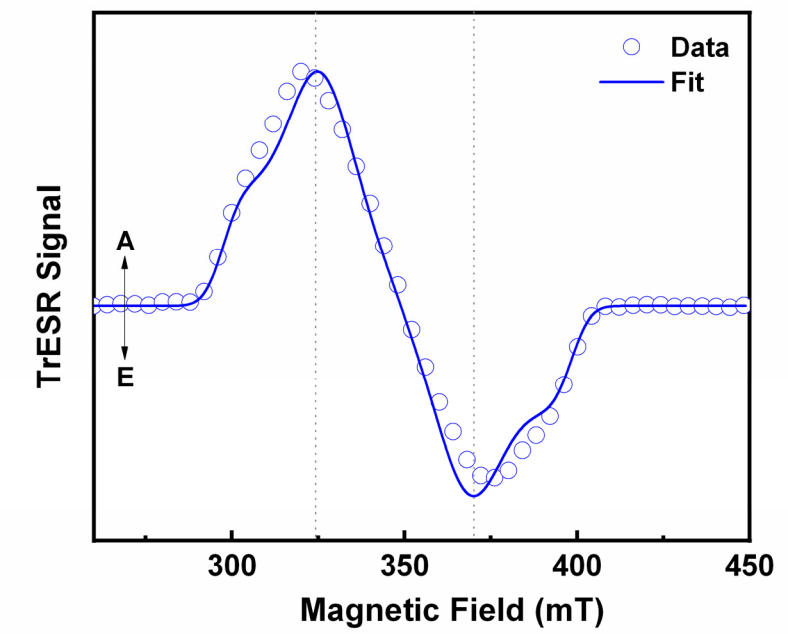

Fig. S9. TrESR spectra at 80 K of 5Cz-TRZ in dilute toluene solutions. The microwave frequency was 9.749 GHz with first 600 ns of time-invariant spectral shape summed. The LASER wavelength was 430 nm at 1 mJ of pulse energy.

Table S2. EPR simulation values for 5Cz-TRZ and TmCz-TRZ.

Molecule	g	D	|E|/|D|	linewidth	P_x	P_y	P_z
5Cz-TRZ	2.0023	1402	0.026	627, 395, 293[a]	0	0.24	0.76

[a]linewidths lw_x,lwy,lw_z in MHz; [b]Distribution of values is derived by multiplying D and E by f (strain).

Transient electron spin resonance (TrESR) is a technique that measures spin polarization following photoexcitation. The TrESR spectrum obtained for 5Cz-TRZ has AAAEEE (A = absorption of microwave, E = emission) polarization patterns that are indicative of triplet, T_1, states formed following intersystem crossing (ISC) mediated by spin-orbit coupling and not hyperfine interactions.[1,2] The triplet spin distributions for these species are oblate, and the zero-field splitting **D** parameter for 5Cz-TRZ is similar to 4CzIPN, which also has an oblate distribution and was found to have mixed CT-LE character.[3]

The 5Cz-TRZ triplet sublevels are preferentially populated following: $P_z > P_y > P_x$. For 4CzIPN, the population ordering follows: $P_y > P_x > P_z$. Like 4CzIPN, 5Cz-TRZ has C_2-rotational axes of symmetry (ignoring torsional fluctuations), and may be ascribed to the C_2 point group. As previous, the static picture for ISC would suggest exclusive population of the P_y sublevel. Consequently, the observed triplet sublevel populations support significant vibronic contributions to ISC for 5Cz-TRZ, such that the P_z level becomes preferentially populated.

Table S3. Photophysical properties of 5Cz-TRZ, mCz-TRZ, TmCz-TRZ and DACT-II in toluene solutions.

Molecule	λ_{em}[a] (nm)	PLQE[a,b,c] (%)	τ_p[a,d] (ns)	τ_d[a,e] (μs)	k_{ISC}[a,f] (s^{-1})	k_{RISC}[a,g] (s^{-1})
5Cz-TRZ	486	92	5.7	1.9	1.7×10^8	1.5×10^7
mCz-TRZ	434	72	5.8	–	–	–
TmCz-TRZ	495	88	20.3	39.1	2.2×10^7	3.3×10^4
DACT-II	526	76	13.1	7.5	1.2×10^7	5.6×10^4

[a]1×10^{-5} M in toluene; [b]Absolute photoluminescence quantum yield (PLQY) by an integrating sphere; [c]Degassed/purged by argon; [d]Prompt lifetime; [e]Delayed lifetime; [f]Intersystem crossing rate constant; [g]Reverse intersystem crossing rate constant.

Table S4. Photophysical properties of 5Cz-TRZ, TmCz-TRZ and DACT-II in 15wt%-doped films.

Molecule	λ_{em}[a] (nm)	PLQE[a,b,c] (%)	τ_p[a,d] (ns)	τ_d[a,e] (μs)	k_{ISC}[a,f] (s^{-1})	k_{RISC}[a,g] (s^{-1})
5Cz-TRZ	486	99	3.0	2.1	3.2×10^8	1.4×10^7
TmCz-TRZ	496	90	14.4	38.0	2.8×10^7	3.9×10^4
DACT-II	530	92	11.7	4.2	1.5×10^7	1.6×10^5

[a]15 wt% doped in mCBP; [b]Absolute photoluminescence quantum yield (PLQY) by an integrating sphere; [c]Degassed/purged by argon; [d]Prompt lifetime; [e]Delayed lifetime; [f]Intersystem crossing rate constant; [g]Reverse intersystem crossing rate constant.

S5. Analysis of k_{ISC} and k_{RISC}

The rate equation for singlet and triplet exciton densities (S_1 and T_1) is described by

$$\frac{d}{dt}\begin{pmatrix} S_1 \\ T_1 \end{pmatrix} = \begin{pmatrix} -(k_r^S + k_{nr}^S + k_{RISC}) & k_{RISC} \\ k_{ISC} & -(k_r^T + k_{nr}^T + k_{RISC}) \end{pmatrix}\begin{pmatrix} S_1 \\ T_1 \end{pmatrix} \quad (1)$$

where k_r^S, k_{nr}^S and k_{ISC} are the rate constants of radiative decay (fluorescence), intrinsic non-radiative decay and ISC for the singlet excitons, respectively. k_r^T, k_{nr}^T and k_{RISC} are the rate constants of radiative decay (phosphorescence), intrinsic non-radiative decay, RISC of the triplet exciton, respectively. The solution of Supplementary equation (1) is given by

$$S_1, T_1 = A_1 exp[-k_p t] + A_2 exp[-k_d t] \quad (2)$$

where A_1 and A_2 are the intensities of the prompt and delayed fluorescence, respectively. The measurable decay rates are the intensities of the prompt and delayed fluorescence, respectively. The measurable decay rates of prompt and delayed fluorescence (k_p and $-k_d$) are thus given by

$$\{(k_r^S + k_{nr}^S + k_{ISC}) - k_p\}\{(k_r^T + k_{nr}^T + k_{RISC}) - k_p\} - k_{ISC}k_{RISC} = 0 \quad (3)$$

$$\{(k_r^S + k_{nr}^S + k_{ISC}) - k_d\}\{(k_r^T + k_{nr}^T + k_{RISC}) - k_d\} - k_{ISC}k_{RISC} = 0 \quad (4)$$

Subtracting and adding Supplementary equations (3) and (4) yield

$$k_p + k_d = k_r^S + k_{nr}^S + k_{ISC} + k_r^T + k_{nr}^T + k_{RISC} \quad (5)$$

$$k_p k_d = (k_r^S + k_{nr}^S + k_{ISC})(k_r^T + k_{nr}^T + k_{RISC}) - k_{ISC}k_{RISC} \quad (6)$$

The PL quantum efficiency of prompt fluorescence (Φ_p) is expressed by

$$\Phi_p = \frac{k_r^S}{k_r^S + k_{nr}^S + k_{ISC}} \quad (7)$$

By assuming (i) $k_p \gg k_d$, (ii) $k_r^S \gg k_{nr}^S$, k_{RISC} and (iii) $k_{RISC} \gg k_r^T, k_{nr}^T$. Supplementary equations (5), (6) and (7) can be simplified to

$$k_p \approx k_r^S + k_{ISC} \tag{8}$$

$$k_p k_d \approx k_r^S k_{RISC} \tag{9}$$

$$\Phi_p \approx \frac{k_r^S}{k_r^S + k_{ISC}} = \frac{k_r^S}{k_p} \tag{10}$$

Solving Supplementary equations (8), (9) and (10) for k_{ISC} yields

$$k_{ISC} \approx k_p - k_r^S = k_p(1 - \Phi_p) \tag{11}$$

Solving Supplementary equations (8) and (10) for k_{RISC} yield

$$k_{RISC} \approx \frac{k_p k_d}{k_p - k_{ISC}} \tag{12}$$

k_{ISC} and k_{RISC} were estimated from Supplementary equations (11) and (12), at which the above assumption seems valid.

S6. Device performance

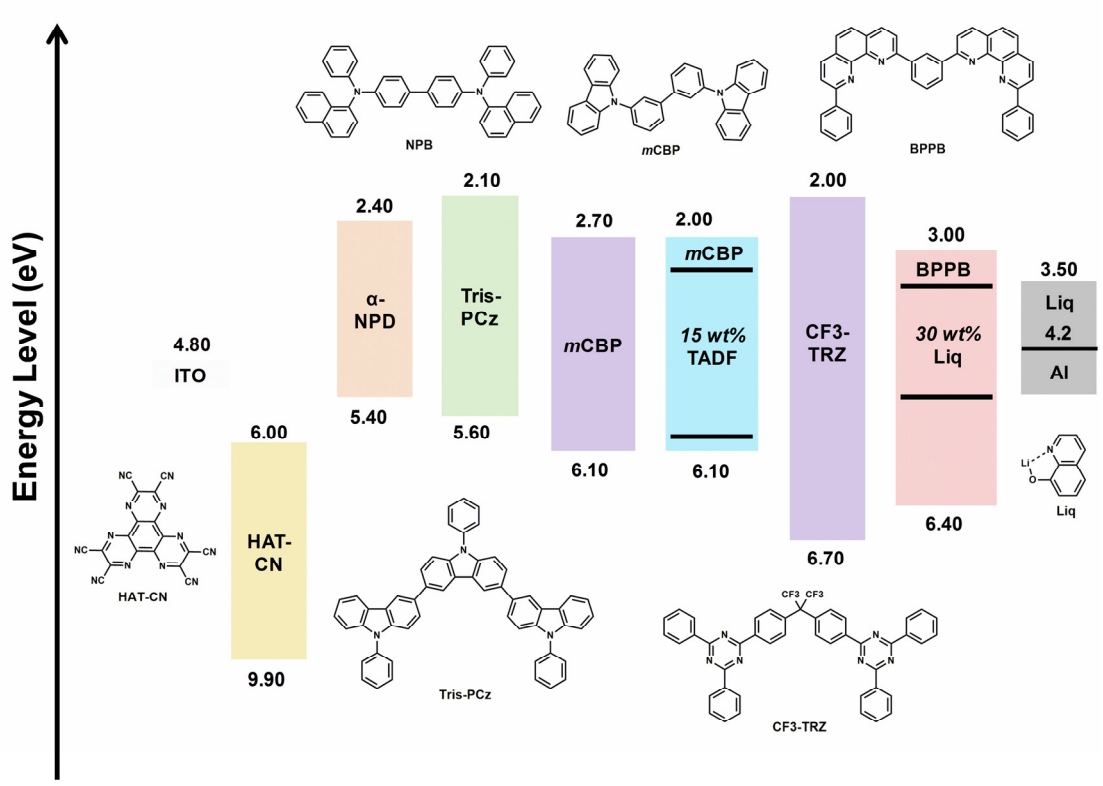

Fig. S10. Energy levels of the materials employed in the devices.

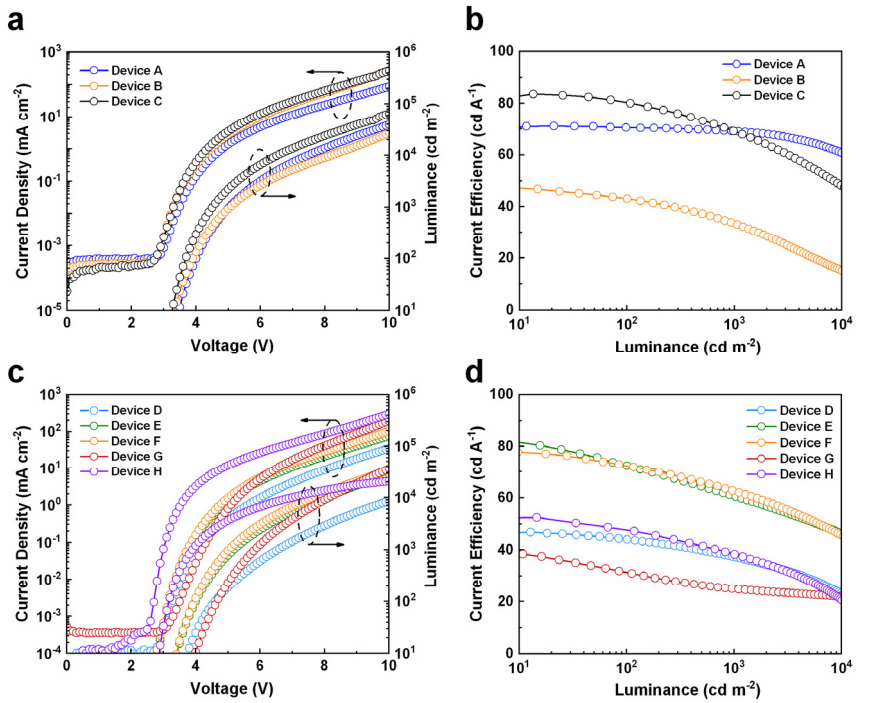

Fig. S11. OLEDs performance. **a,** *J-V-L* characteristics of Device A, B and C. **b,** Current efficiency versus luminance characteristics of Device A, B and C. **d,** *J -V-L* characteristics of Device D, E, F and G. **d,** Current efficiency versus luminance characteristics of Device D, E, F and G.

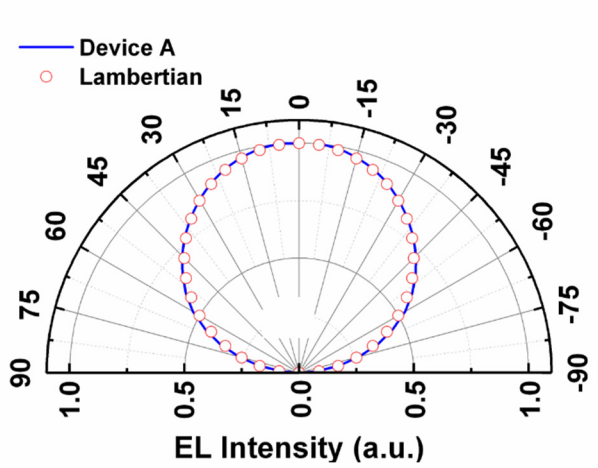

Fig. S12. The angular distribution of the EL intensity for the Device A.

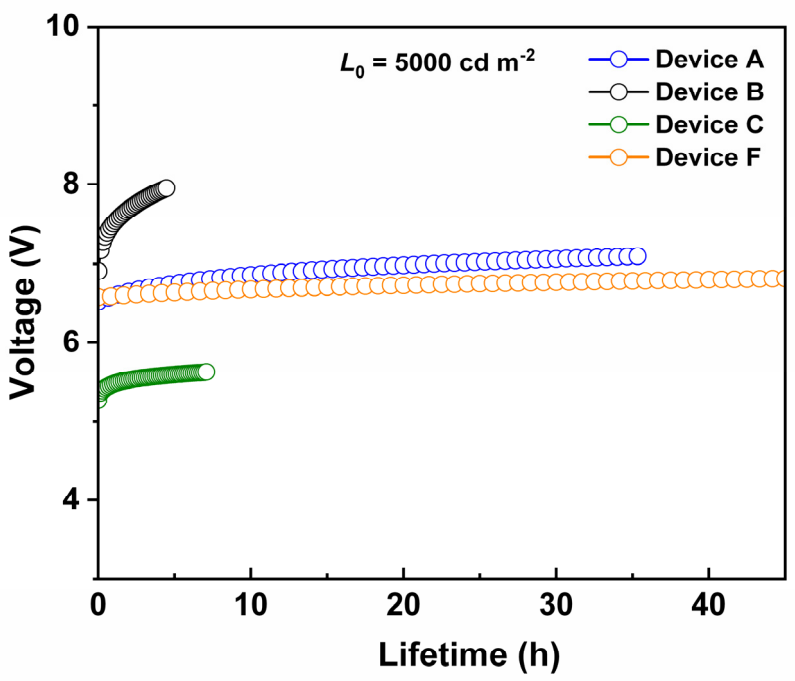

Fig. S13. Changes in voltage of the devices A, B, C and F device versus operational time during which the devices driven at an initial luminescence of 5,000 cd cm^{-2}.

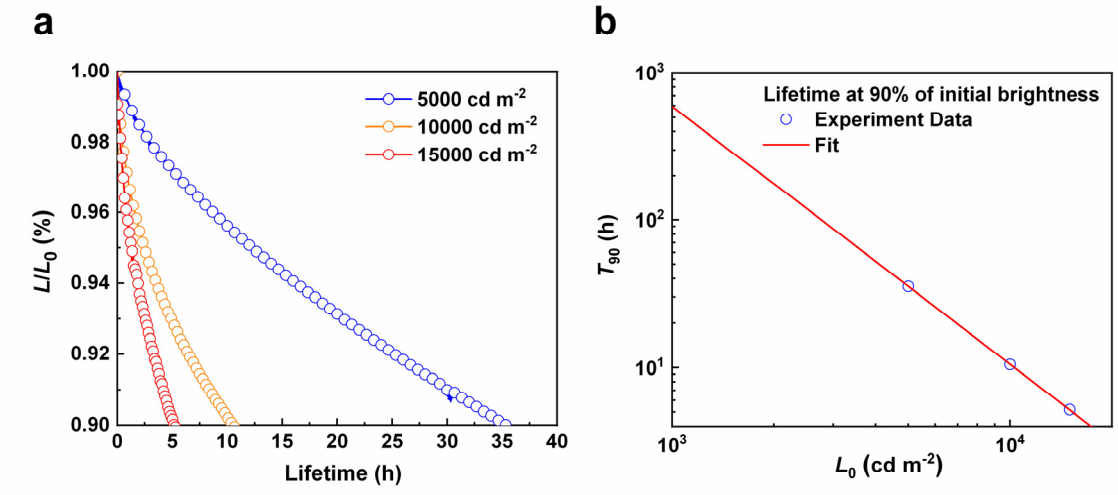

Fig. S14. Operational lifetimes of device A at different initial brightness levels. **a,** Operational lifetimes of device A at the initial brightness of 15,000, 10,000 and 5,000 cd m^{-2}. **b,** Log–log plot of T_{90} with initial brightness, we estimated the T_{90} at an initial brightness of 1000 cd m^{-2} to be 592.2 h.

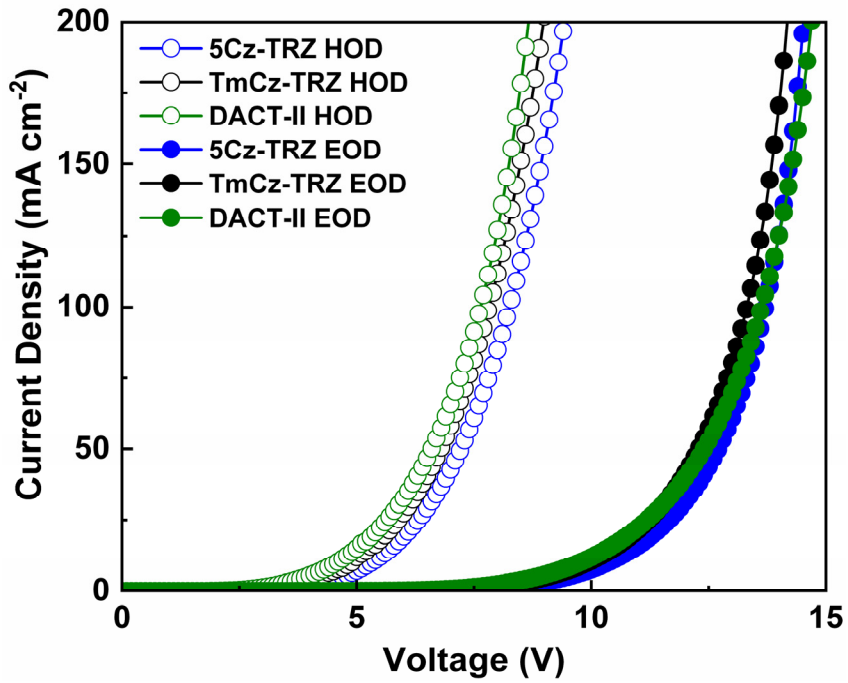

Fig. S15. *J–V* curves for the hole-only devices (ITO/ HAT-CN (10 nm)/ α-NPD (30 nm)/ Tris-PCz (10 nm)/ *m*CBP (6 nm)/ 15 wt% TADF: mCBP (20 nm)/ Tris-PCz (20 nm)/ Al (100 nm)) and the electron-only devices (ITO/PO-T2T (20 nm)/ 15 wt% TADF: mCBP (20 nm)/ CF3-TRZ (10 nm)/ 30 wt% Liq: BPPB (45 nm)/Liq (2 nm)/Al (120 nm)).

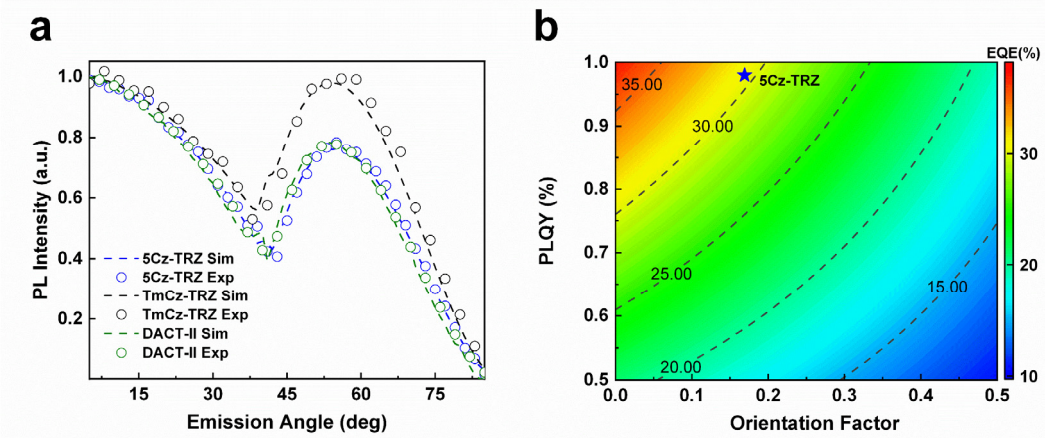

Fig. S16. a, Variable-angle PL measurements of 15 wt% 5Cz-TRZ, 15 wt% TmCz-TRZ and 15 wt% DACT-II in mCBP doped films, which were fitted with orientation factors of 0.17, 0.26 and 0.18, respectively. **b,** Calculated maximum EQE according to the molecular orientation factor and PLQE of 5Cz-TRZ. The blue star indicates the maximum EQE obtained from the experiment.

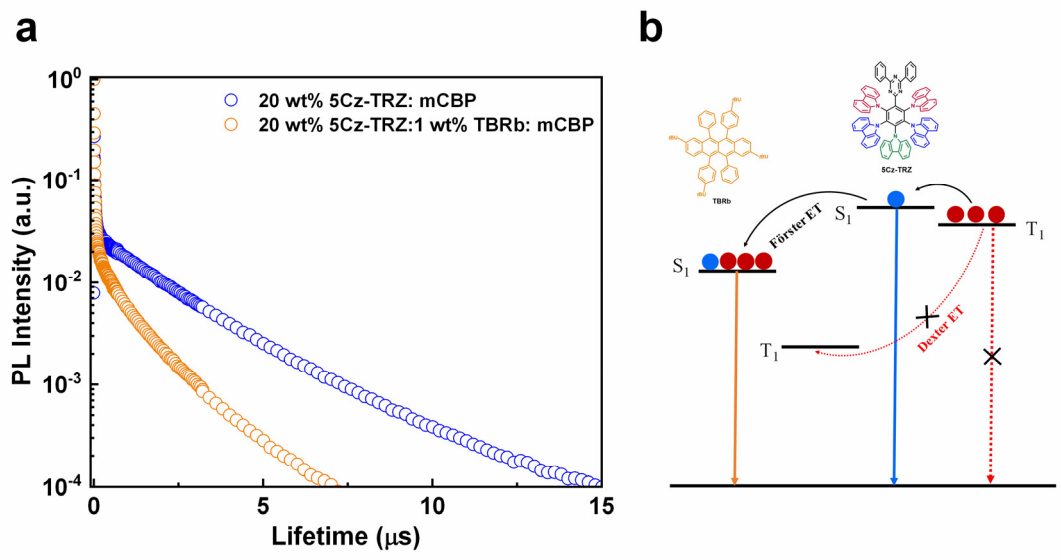

Fig. S17. a, Time-resolved PL (300 K) measurements of hyperfluorescence system. **b,** Energy transfer mechanism in the hyperfluorescence system.

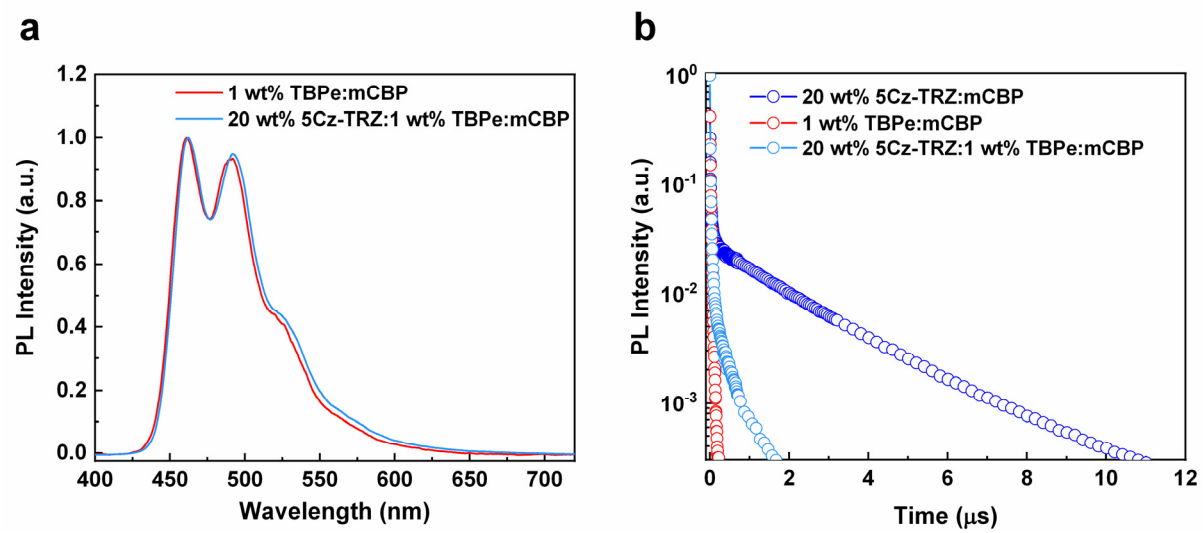

Fig. S18. a, PL spectra for the 1 wt% TBPe: mCBP and 20 wt% 5Cz-TRZ: 1 wt% TBPe: mCBP co-deposited films. **b,** Time-resolved PL (300 K) measurements for the 20 wt% 5Cz-TRZ: mCBP, 1 wt% TBPe: mCBP and 20 wt% 5Cz-TRZ: 1 wt% TBPe: mCBP co-deposited films.

Table S5. Summary performance of the state-of-the-art TADF-based OLEDs

Emitter	EL (nm)	EQE_{max} (%)	$EQE_{@1000}$ (%)	Eff. Roll-off (%)	T_{90}@ initial brightness (h)	Ref.
5Cz-TRZ	**486**	**29.3**	**28.6**	**2.4**	**35.4@5000 cd m^{-2}**	**this work**
SpiroAC-TRZ	483	36.7	30.5	16.7	−	4
BuCzMeoB	479	32.8	18.5	43.6	−	5
2SPAc-PPM	484	31.5	10.8	65.7	−	6
5TCzBN	490	21.2	9.2	56.6	80@500 cd m^{-2}	7
BCz-TRZ	486	20.5	16.2	21.0	2@500 cd m^{-2}	8
DMAC-TRZ	495	26.5	20.2	23.8	−	9
DDCzTrz	476	18.9	4	78.8	20@500 cd m^{-2}	10
TBN-TPA	475	32.1	13.9	56.7	−	11
TZ-SBA	490	35.2	26.7	24.1	−	12
Ac-MPM	482	24.5	10.1	58.7	−	13
TDBA–DI	480	38.2	34.3	10.2	−	14
ν-DABNA	470	31.0	23.2	25.2	2@100 cd m^{-2}	15
$3Ph_2CzCzBN$	482	17.8	16.6	6.7	38@1000 cd m^{-2}	16
TAT-3DBTO2	504	30.9	16.5	46.6	−	17
TpAT-tFFO	495	19.2	18.1	5.7	−	18

S7. X-ray structural analysis

The single crystal of 5Cz-TRZ was achieved from the solvent diffusion method with dichloromethane and methanol. Single-crystal X-ray-diffraction data were obtained from were collected at Beamline I19 of Diamond Light Source employing silicon double crystal monochromatic synchrotron radiation (0.6889 Å) with ω and ψ scans at 100(2) K.[19] Data integration and reduction were undertaken with Xia.[20,21,22] Subsequent computations were carried out using the WinGX-32 graphical user interface.[23] A multi-scan empirical absorption correction was applied to the data using the AIMLESS tool in the CCP4 suite.[24,25] The structure was solved by direct methods using SHELXT then refined and extended with SHELXL.[26,27] In general, non-hydrogen atoms with occupancies greater than 0.5 were refined anisotropically. Carbon-bound hydrogen atoms were included in idealised positions and refined using a riding model. Disorder was modelled using standard crystallographic methods including constraints and restraints where necessary. Oxygen-bound hydrogen atoms were first located in the difference Fourier map before refinement. The hydrogen atoms of one of the low occupancy disordered methanol solvent molecules could not be located in the electron density map and were therefore not included in the model. One of the carbazole substituents on one of the two crystallographically unique molecules was modelled as disordered over two locations of approximately equal occupancy. The X-ray crystallographic data for 5Cz-TRZ have been deposited at the Cambridge Crystallographic Data Centre (CCDC) under the deposited number CCDC 1967941.

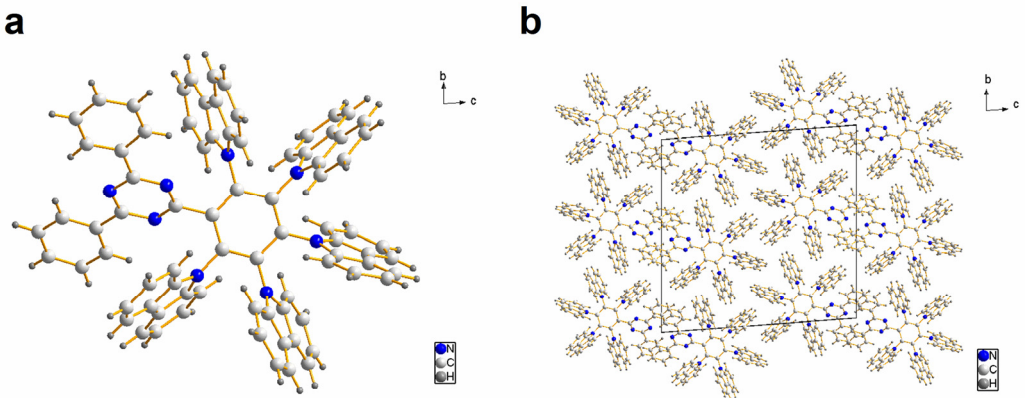

Fig. S19. Crystal structure **a,** ORTEP image of 5Cz-TRZ. **b,** Packing pattern (view along *a* axis) of 5Cz-TRZ.

Table S6. Crystallographic data for 5Cz-TRZ.

Compound	**5Cz-TRZ**
Empirical formula	$C_{82.70}H_{56.20}Cl_{0.60}N_8O_{1.40}$
Formula weight	1205.62
Temperature/K	100(2)
Wavelength/Å	0.6889
Crystal system	Triclinic
Space group	P -1
a/Å	9.71426(3)
b/Å	24.74806(6)
c/Å	25.30621(6)
α/°	85.1315(2)
β/°	80.7019(2)
γ/°	85.6526(2)°
Volume/Å^3	5970.31(3)
Z	4
ρ_{calc}g/cm^3	1.341
μ/mm^{-1}	0.098
F(000)	2519
Crystal size/mm^3	0.200 × 0.020 × 0.010
2Θ range for data collection/°	1.584 to 64.000
Index ranges	-14 ≤ h ≤ 14, -38 ≤ k ≤ 38, -38 ≤ l ≤ 38
Reflections collected	117338
Independent reflections	44207 [R(int) = 0.0432]
Completeness to theta = 24.415°	99.2 %
Max. and min. transmission	1.0 and 0.989410707387
Refinement method	Full-matrix least-squares on F^2
Data/restraints/parameters	44207/641/1870
Goodness-of-fit on F^2	1.105
Final R indexes [I>=2σ (I)]	R1 = 0.0518, wR2 = 0.1460
Final R indexes [all data]	R1 = 0.0667, wR2 = 0.1533
Largest diff. peak/hole / e Å^{-3}	0.465 and -0.352 e.Å^{-3}

Table S7. Atomic coordinates ($\times 10^4$) and equivalent isotropic displacement parameters ($Å^2 \times 10^3$) for 5Cz-TRZ. U(eq) is defined as one third of the trace of the orthogonalized U^{ij} tensor.

	x	y	z	U(eq)
N(1)	7153(1)	4790(1)	532(1)	22(1)
N(2)	6045(1)	4206(1)	1242(1)	19(1)
N(3)	7856(1)	4746(1)	1391(1)	20(1)
N(4)	6926(1)	3246(1)	1882(1)	17(1)
N(5)	6691(1)	2879(1)	2975(1)	17(1)
N(6)	6230(1)	3640(1)	3773(1)	17(1)
N(7)	6057(1)	4763(1)	3467(1)	17(1)
N(8)	6318(1)	5127(1)	2372(1)	18(1)
N(10)	2415(1)	283(1)	9434(1)	21(1)
N(11)	1456(1)	788(1)	8725(1)	23(1)
N(12)	3602(1)	253(1)	8538(1)	21(1)
N(13)	2425(1)	1734(1)	8054(1)	21(1)
N(14)	2773(1)	2095(1)	6960(1)	27(1)
N(15)	3045(1)	1332(1)	6170(1)	20(1)
N(16)	3176(1)	208(1)	6481(1)	19(1)
N(17)	2947(1)	-155(1)	7571(1)	18(1)
C(1)	6278(1)	4401(1)	722(1)	19(1)
C(2)	6870(1)	4390(1)	1549(1)	18(1)
C(3)	7903(1)	4959(1)	879(1)	19(1)
C(4)	5521(1)	4176(1)	339(1)	20(1)
C(5)	5710(1)	4380(1)	-200(1)	24(1)
C(6)	5020(1)	4163(1)	-564(1)	27(1)
C(7)	4147(1)	3742(1)	-399(1)	28(1)

C(8)	3959(1)	3537(1)	136(1)	27(1)
C(9)	4640(1)	3752(1)	505(1)	23(1)
C(10)	8859(1)	5395(1)	691(1)	21(1)
C(11)	9498(1)	5645(1)	1052(1)	24(1)
C(12)	10439(1)	6039(1)	864(1)	28(1)
C(13)	10737(1)	6188(1)	321(1)	28(1)
C(14)	10078(1)	5951(1)	-39(1)	27(1)
C(15)	9138(1)	5556(1)	142(1)	25(1)
C(16)	6688(1)	4187(1)	2128(1)	16(1)
C(17)	6754(1)	3629(1)	2280(1)	16(1)
C(18)	6618(1)	3443(1)	2826(1)	15(1)
C(19)	6394(1)	3822(1)	3221(1)	16(1)
C(20)	6297(1)	4383(1)	3070(1)	16(1)
C(21)	6448(1)	4562(1)	2523(1)	16(1)
C(22)	8139(1)	3129(1)	1520(1)	18(1)
C(23)	9480(1)	3297(1)	1503(1)	20(1)
C(24)	10518(1)	3099(1)	1109(1)	24(1)
C(25)	10228(1)	2748(1)	742(1)	27(1)
C(26)	8884(1)	2592(1)	753(1)	24(1)
C(27)	7818(1)	2785(1)	1144(1)	19(1)
C(28)	6338(1)	2705(1)	1276(1)	19(1)
C(29)	5408(1)	2429(1)	1042(1)	24(1)
C(30)	4008(1)	2456(1)	1262(1)	25(1)
C(31)	3518(1)	2753(1)	1710(1)	25(1)
C(32)	4420(1)	3027(1)	1949(1)	22(1)
C(33)	5826(1)	2997(1)	1729(1)	18(1)
C(34)	7924(1)	2541(1)	2934(1)	16(1)

C(35)	9292(1)	2673(1)	2753(1)	20(1)
C(36)	10333(1)	2262(1)	2790(1)	23(1)
C(37)	10024(1)	1736(1)	2995(1)	26(1)
C(38)	8654(1)	1605(1)	3165(1)	23(1)
C(39)	7588(1)	2012(1)	3137(1)	18(1)
C(40)	6091(1)	2024(1)	3299(1)	17(1)
C(41)	5170(1)	1625(1)	3508(1)	21(1)
C(42)	3755(1)	1770(1)	3617(1)	22(1)
C(43)	3253(1)	2309(1)	3521(1)	22(1)
C(44)	4147(1)	2714(1)	3313(1)	20(1)
C(45)	5570(1)	2565(1)	3202(1)	16(1)
C(46)	7286(1)	3420(1)	4061(1)	18(1)
C(47)	8701(1)	3313(1)	3881(1)	21(1)
C(48)	9523(1)	3103(1)	4261(1)	25(1)
C(49)	8968(1)	3020(1)	4805(1)	27(1)
C(50)	7559(1)	3125(1)	4979(1)	24(1)
C(51)	6692(1)	3313(1)	4601(1)	19(1)
C(52)	5201(1)	3434(1)	4637(1)	19(1)
C(53)	4061(1)	3337(1)	5040(1)	25(1)
C(54)	2728(1)	3478(1)	4927(1)	27(1)
C(55)	2518(1)	3727(1)	4427(1)	24(1)
C(56)	3628(1)	3817(1)	4016(1)	21(1)
C(57)	4959(1)	3652(1)	4125(1)	17(1)
C(58)	6982(1)	4836(1)	3824(1)	18(1)
C(59)	8372(1)	4649(1)	3804(1)	22(1)
C(60)	9077(1)	4804(1)	4198(1)	26(1)
C(61)	8410(1)	5131(1)	4599(1)	29(1)

C(62)	7024(1)	5312(1)	4618(1)	26(1)
C(63)	6297(1)	5169(1)	4222(1)	19(1)
C(64)	4900(1)	5302(1)	4106(1)	19(1)
C(65)	3746(1)	5604(1)	4364(1)	26(1)
C(66)	2518(1)	5647(1)	4151(1)	29(1)
C(67)	2425(1)	5403(1)	3681(1)	27(1)
C(68)	3554(1)	5099(1)	3417(1)	22(1)
C(69)	4783(1)	5051(1)	3638(1)	18(1)
C(70)	7306(1)	5504(1)	2402(1)	20(1)
C(71)	8591(1)	5421(1)	2577(1)	24(1)
C(72)	9386(1)	5871(1)	2546(1)	29(1)
C(73)	8915(1)	6385(1)	2341(1)	33(1)
C(74)	7630(1)	6461(1)	2171(1)	30(1)
C(75)	6803(1)	6018(1)	2203(1)	23(1)
C(76)	5447(1)	5954(1)	2061(1)	23(1)
C(77)	4392(1)	6318(1)	1896(1)	31(1)
C(78)	3151(1)	6121(1)	1824(1)	36(1)
C(79)	2950(1)	5563(1)	1892(1)	32(1)
C(80)	3976(1)	5192(1)	2054(1)	24(1)
C(81)	5198(1)	5396(1)	2154(1)	20(1)
C(101)	1460(1)	635(1)	9249(1)	20(1)
C(102)	2577(1)	598(1)	8396(1)	21(1)
C(103)	3436(1)	86(1)	9066(1)	19(1)
C(104)	321(1)	857(1)	9647(1)	20(1)
C(105)	198(1)	654(1)	10186(1)	27(1)
C(106)	-883(1)	853(1)	10559(1)	29(1)
C(107)	-1844(1)	1252(1)	10404(1)	27(1)

C(108)	-1720(1)	1459(1)	9872(1)	26(1)
C(109)	-638(1)	1264(1)	9493(1)	22(1)
C(110)	4424(1)	-345(1)	9248(1)	20(1)
C(111)	5378(1)	-623(1)	8877(1)	21(1)
C(112)	6272(1)	-1040(1)	9056(1)	26(1)
C(113)	6221(1)	-1180(1)	9602(1)	28(1)
C(114)	5269(1)	-906(1)	9971(1)	28(1)
C(115)	4366(1)	-493(1)	9798(1)	25(1)
C(116)	2698(1)	788(1)	7814(1)	20(1)
C(117)	2647(1)	1347(1)	7659(1)	20(1)
C(118)	2789(1)	1531(1)	7112(1)	21(1)
C(119)	2949(1)	1151(1)	6721(1)	20(1)
C(120)	3000(1)	590(1)	6874(1)	19(1)
C(121)	2881(1)	412(1)	7423(1)	19(1)
C(122)	3334(1)	1826(1)	8408(1)	27(1)
C(123)	4708(1)	1625(1)	8418(1)	39(1)
C(124)	5390(2)	1807(1)	8804(1)	57(1)
C(125)	4744(2)	2170(1)	9171(1)	63(1)
C(126)	3370(2)	2357(1)	9167(1)	52(1)
C(127)	2643(1)	2183(1)	8784(1)	31(1)
C(128)	1246(1)	2294(1)	8668(1)	28(1)
C(129)	65(2)	2585(1)	8918(1)	40(1)
C(130)	-1169(2)	2589(1)	8717(1)	46(1)
C(131)	-1252(1)	2305(1)	8269(1)	39(1)
C(132)	-99(1)	2009(1)	8013(1)	27(1)
C(133)	1139(1)	2009(1)	8217(1)	21(1)
C(134)	3744(6)	2431(3)	6935(3)	22(1)

C(135)	4992(6)	2334(2)	7137(3)	27(1)
C(136)	5898(5)	2756(2)	7061(2)	34(1)
C(137)	5555(5)	3255(2)	6793(2)	36(1)
C(138)	4293(5)	3347(2)	6606(2)	33(1)
C(139)	3361(5)	2936(1)	6674(2)	23(1)
C(140)	2003(4)	2894(2)	6533(2)	24(1)
C(141)	1071(6)	3273(1)	6301(1)	33(1)
C(142)	-192(5)	3098(2)	6231(1)	37(1)
C(143)	-561(4)	2564(2)	6389(2)	32(1)
C(144)	327(5)	2190(2)	6627(2)	24(1)
C(145)	1599(5)	2365(2)	6695(2)	20(1)
C(234)	4073(7)	2410(3)	6978(4)	22(1)
C(235)	5304(7)	2256(3)	7170(4)	26(1)
C(236)	6326(6)	2633(2)	7104(2)	33(1)
C(237)	6111(6)	3150(2)	6853(2)	37(1)
C(238)	4874(6)	3306(2)	6663(2)	33(1)
C(239)	3843(5)	2931(2)	6722(2)	25(1)
C(240)	2489(5)	2947(2)	6561(2)	25(1)
C(241)	1674(6)	3350(2)	6314(2)	36(1)
C(242)	366(6)	3243(2)	6228(2)	40(1)
C(243)	-161(5)	2734(2)	6372(2)	39(1)
C(244)	624(6)	2321(2)	6630(2)	29(1)
C(245)	1937(6)	2435(2)	6715(3)	23(1)
C(146)	4180(1)	1580(1)	5856(1)	19(1)
C(147)	5482(1)	1661(1)	5980(1)	22(1)
C(148)	6463(1)	1877(1)	5572(1)	25(1)
C(149)	6155(1)	2005(1)	5052(1)	25(1)

C(150)	4837(1)	1946(1)	4936(1)	23(1)
C(151)	3830(1)	1735(1)	5342(1)	19(1)
C(152)	2407(1)	1597(1)	5353(1)	20(1)
C(153)	1473(1)	1687(1)	4984(1)	25(1)
C(154)	145(1)	1503(1)	5124(1)	30(1)
C(155)	-250(1)	1226(1)	5624(1)	32(1)
C(156)	639(1)	1143(1)	6001(1)	28(1)
C(157)	1967(1)	1336(1)	5862(1)	21(1)
C(158)	4416(1)	82(1)	6132(1)	19(1)
C(159)	5738(1)	273(1)	6107(1)	21(1)
C(160)	6806(1)	60(1)	5733(1)	24(1)
C(161)	6567(1)	-334(1)	5397(1)	24(1)
C(162)	5242(1)	-511(1)	5416(1)	23(1)
C(163)	4146(1)	-298(1)	5784(1)	19(1)
C(164)	2670(1)	-385(1)	5905(1)	20(1)
C(165)	1776(1)	-669(1)	5666(1)	25(1)
C(166)	363(1)	-649(1)	5873(1)	28(1)
C(167)	-157(1)	-360(1)	6323(1)	26(1)
C(168)	707(1)	-76(1)	6570(1)	23(1)
C(169)	2114(1)	-81(1)	6346(1)	19(1)
C(170)	4178(1)	-488(1)	7542(1)	17(1)
C(171)	5548(1)	-355(1)	7366(1)	20(1)
C(172)	6595(1)	-762(1)	7413(1)	23(1)
C(173)	6290(1)	-1290(1)	7622(1)	23(1)
C(174)	4921(1)	-1421(1)	7791(1)	20(1)
C(175)	3852(1)	-1017(1)	7755(1)	17(1)
C(176)	2356(1)	-1002(1)	7923(1)	19(1)

C(177)	1432(1)	-1396(1)	8146(1)	25(1)
C(178)	27(1)	-1245(1)	8265(1)	33(1)
C(179)	-469(1)	-706(1)	8169(1)	39(1)
C(180)	425(1)	-306(1)	7945(1)	33(1)
C(181)	1836(1)	-461(1)	7817(1)	21(1)
Cl(2)	7702(2)	689(1)	8579(1)	42(1)
Cl(1)	7523(1)	932(1)	7442(1)	44(1)
C(1S)	7089(4)	482(1)	8014(2)	32(1)
O(10S)	8574(2)	841(1)	8377(1)	24(1)
C(10S)	7753(5)	465(2)	8727(1)	29(1)
C(11S)	7750(3)	1096(2)	7091(1)	63(1)
O(11S)	8942(2)	955(1)	7286(1)	38(1)
Cl(4)	11043(2)	4049(1)	2540(1)	53(1)
Cl(3)	12064(2)	4332(1)	1399(1)	45(1)
C(2S)	10884(6)	4509(2)	1972(3)	40(1)
C(13S)	11637(2)	4476(1)	1280(1)	34(1)
O(13S)	10618(1)	4567(1)	1737(1)	26(1)
O(12S)	10281(2)	3968(1)	2693(1)	33(1)
C(12S)	11459(2)	4026(1)	2939(1)	42(1)
O(15S)	6613(9)	1019(3)	7295(4)	64(2)
C(15S)	7911(13)	775(6)	7161(7)	71(4)
C(14S)	7360(15)	561(10)	8672(6)	37(4)
O(14S)	6762(9)	440(4)	8232(3)	50(2)

S8. NMR spectra

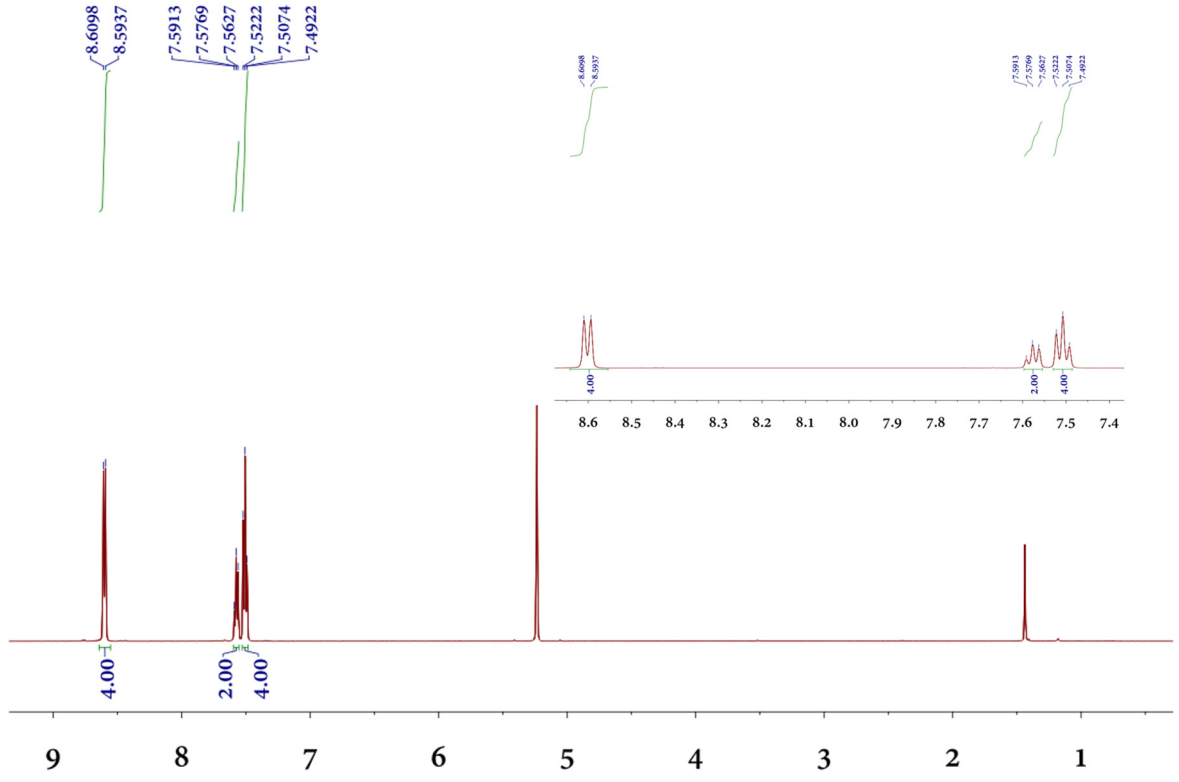

Fig. S20. [1]H NMR spectrum of 2-(perfluorophenyl)-4,6-diphenyl-1,3,5-triazine.

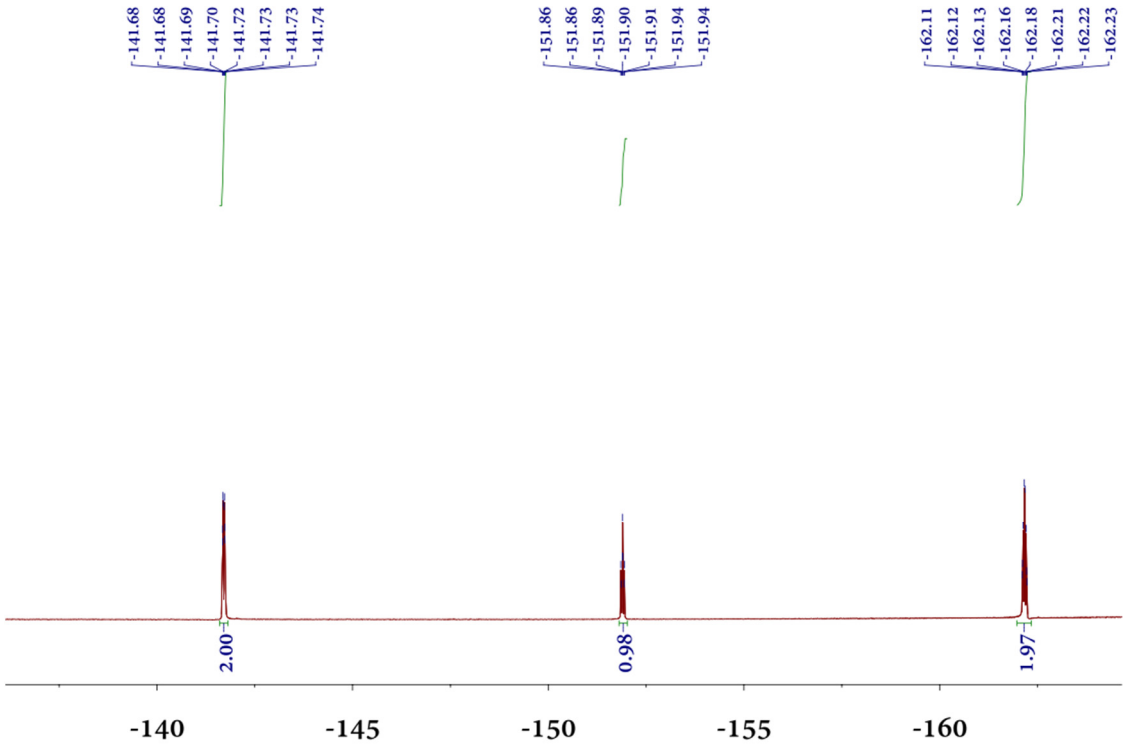

Fig. S21. [19]F NMR spectrum of 2-(perfluorophenyl)-4,6-diphenyl-1,3,5-triazine.

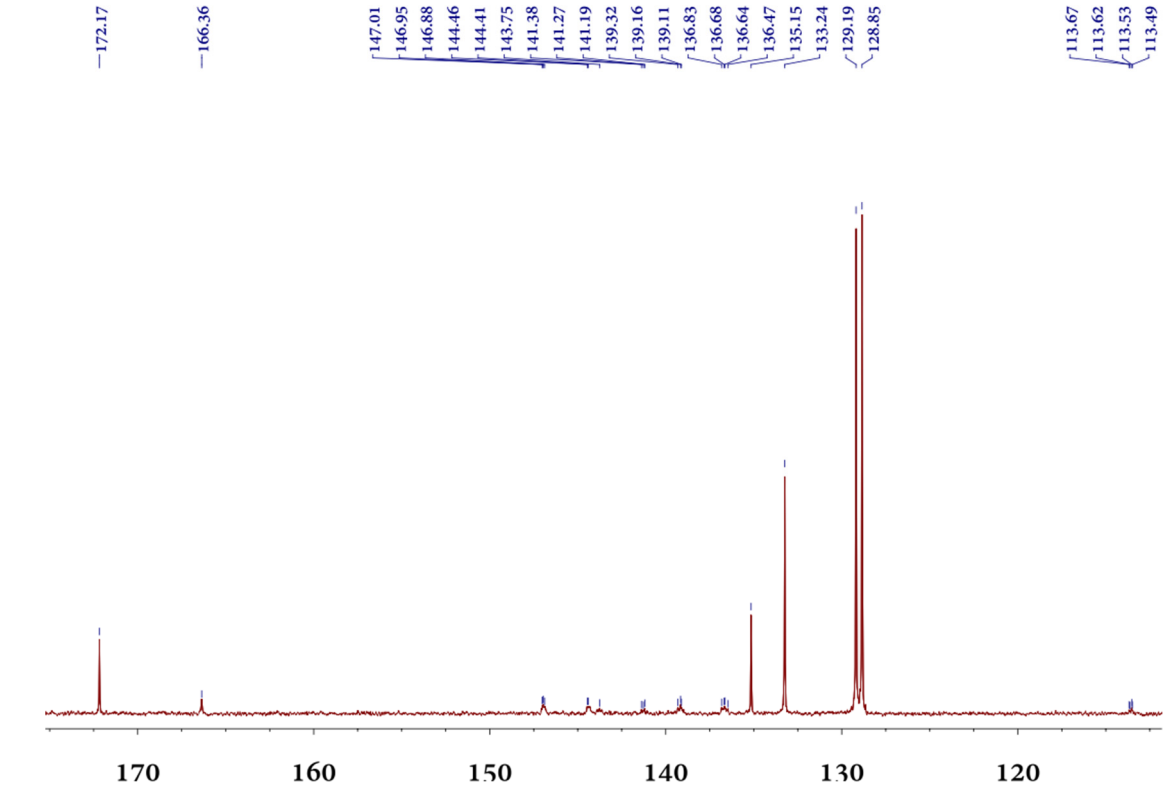

Fig. S22. ^{13}C NMR spectrum of 2-(perfluorophenyl)-4,6-diphenyl-1,3,5-triazine.

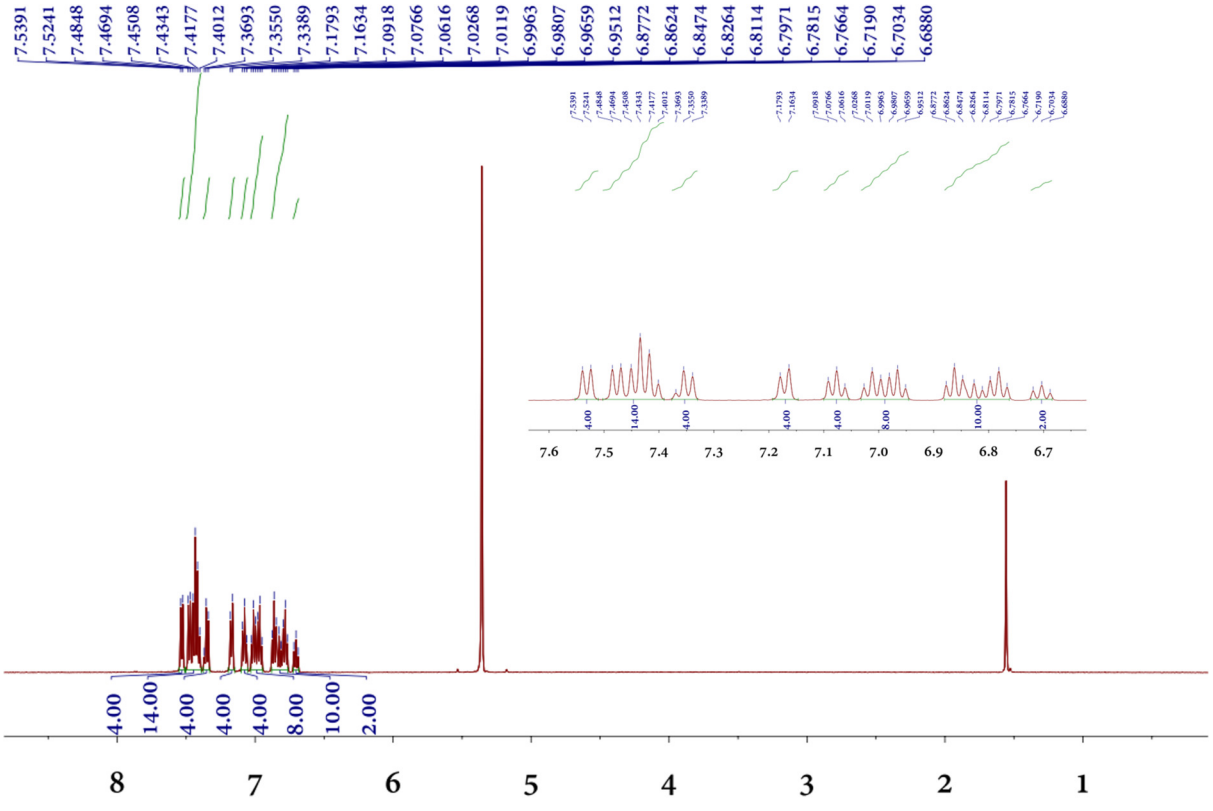

Fig. S23. ^{1}H NMR spectrum of 5Cz-TRZ.

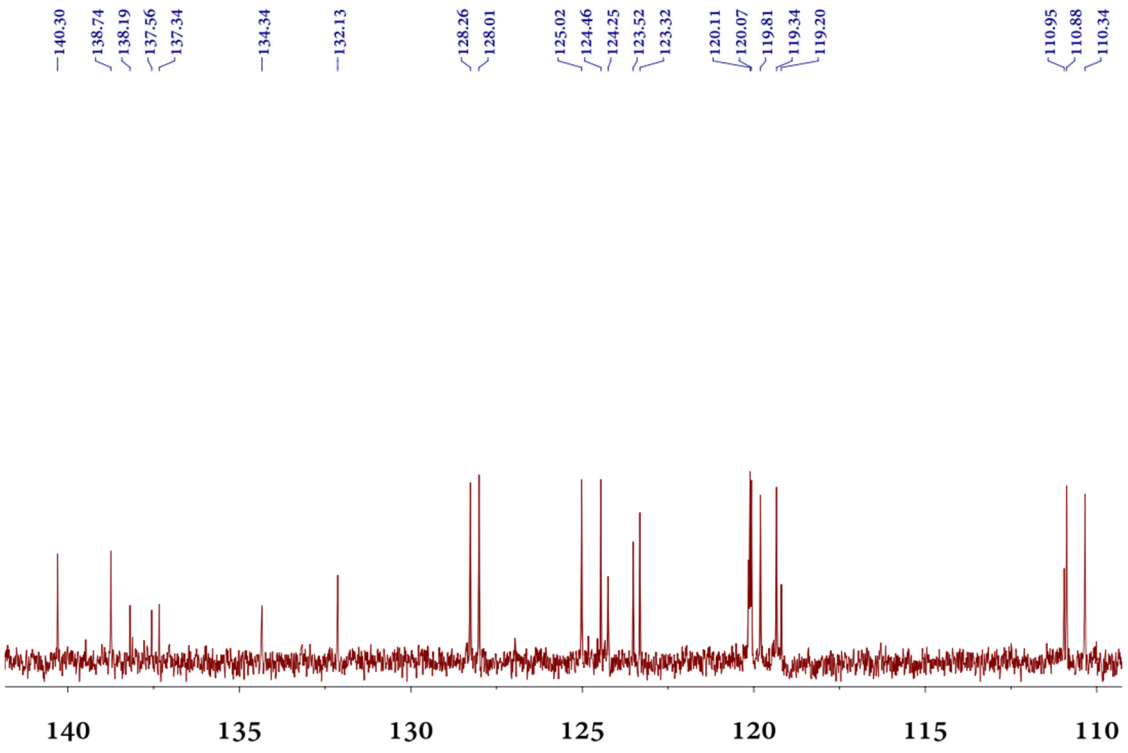

Fig. S24. ^{13}C NMR spectrum of 5Cz-TRZ.

S9. HPLC chromatogram

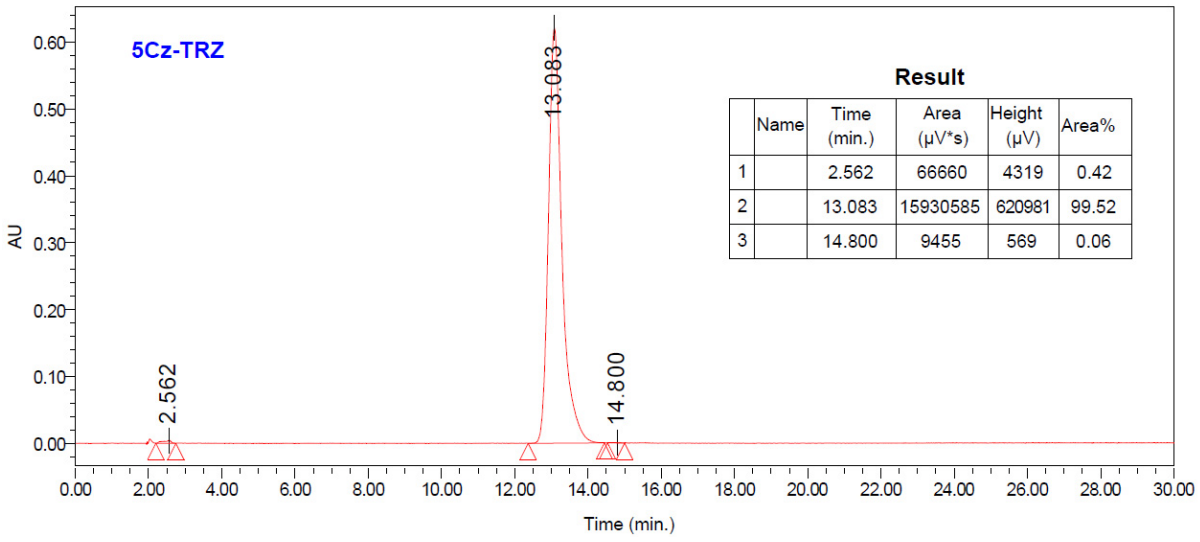

Fig. S25. Purity of 5Cz-TRZ (99.52%) by HPLC.

S10. Mass spectrum

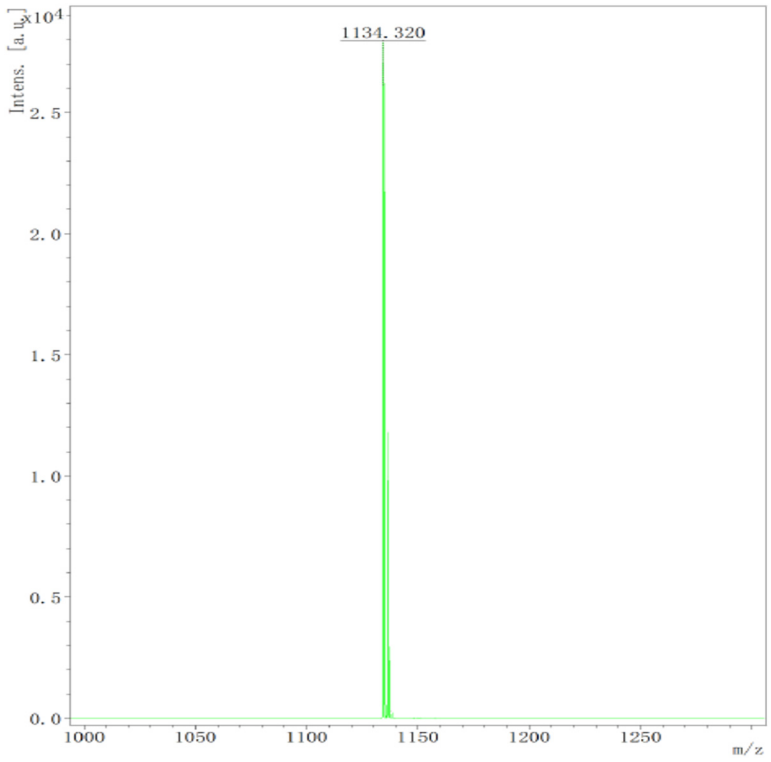

Fig. S26. Mass spectrum of 5Cz-TRZ.

S11. References

1. Hoff, A. J. Advanced EPR: Applications in Biology and Biochemistry. Elseveier: Amsterdam (1989).
2. Ogiwara, T., Wakikawa, Y. & Ikoma, T. Mechanism of intersystem crossing of thermally activated delayed fluorescence molecules. *J. Phys. Chem. A* **119,** 3415–3418 (2015).
3. Evans, E. W. et al. Vibrationally assisted intersystem crossing in benchmark thermally activated delayed fluorescence molecules. *J. Phys. Chem. Lett.* **9,** 4053–4058 (2018).
4. Lin, T. A. et al. Sky-blue organic light emitting diode with 37% external quantum efficiency using thermally activated delayed fluorescence from spiroacridine-triazine hybrid. *Adv. Mater.* **28,** 6976–6983 (2016).
5. Lee, Y. H. et al. High-efficiency sky blue to ultra-deep blue thermally activated delayed fluorescent diodes based on ortho-carbazole-appended triarylboron emitters: above 32% external quantum efficiency in blue devices. *Adv. Opt. Mater.* **6,** 1800385 (2018).

6. Li, B. et al. Highly efficient blue organic light-emitting diodes from pyrimidine-based thermally activated delayed fluorescence emitters. *J. Mater. Chem. C.* **6,** 2351–2359 (2018).
7. Zhang, D. et al. Sterically shielded blue thermally activated delayed fluorescence emitters with improved efficiency and stability. *Mater. Horiz.* **3,** 145–151 (2016).
8. Cui, L. -S. et al. Controlling synergistic oxidation processes for efficient and stable blue thermally activated delayed fluorescence devices. *Adv. Mater.* **28,** 7620–7625 (2016).
9. Tsai, W. L. et al. A versatile thermally activated delayed fluorescence emitter for both highly efficient doped and non-doped organic light emitting devices. *Chem. Commun.* **51,** 13662–13665 (2015).
10. Kim, M., Jeon, S. K., Hwang, S. H. & Lee, J. Y. Stable blue thermally activated delayed fluorescent organic light-emitting diodes with three times longer lifetime than phosphorescent organic light-emitting diodes. *Adv. Mater.* **27,** 2515–2520 (2015).
11. Liang, X. et al. Peripheral Amplification of Multi-resonance induced thermally activated delayed fluorescence for highly efficient OLEDs. *Angew. Chem. Int. Ed.* **57,** 11316–11320 (2018).
12. Liu, M. et al. Horizontally Orientated Sticklike Emitters: Enhancement of intrinsic out-coupling factor and electroluminescence performance. *Chem. Mater.* **29,** 8630–8636 (2017).
13. Komatsu, R., Sasabe, H., Seino, Y., Nakao, K. & Kido, J. Light-blue thermally activated delayed fluorescent emitters realizing a high external quantum efficiency of 25% and unprecedented low drive voltages in OLEDs. *J. Mater. Chem. C,* **4,** 2274–2278 (2016)
14. Ahn, D. H. et al. Highly efficient blue thermally activated delayed fluorescence emitters based on symmetrical and rigid oxygen-bridged boron acceptors. *Nat. Photon.* **13,** 540–546 (2019)
15. Kondo1, Y. et al. Narrowband deep-blue organic light-emitting diode featuring an organoboron-based emitter. *Nat. Photon.* **13,** 678–682 (2019).
16. Chan, C.-Y. et al. Efficient and stable sky-blue delayed fluorescence organic light-emitting diodes with CIEy below 0.4. *Nat. Commun.* **9,** 5036 (2018).
17. Santos, P. L. dos et al. Triazatruxene: A rigid central donor unit for a D-A_3 thermally activated delayed fluorescence material exhibiting sub-microsecond reverse intersystem crossing and unity quantum yield via multiple singlet-triplet state pairs. *Adv. Sci.* **5,** 1700989 (2018).
18. Wada, Y., Nakagawa, H., Matsumoto, S., Wakisaka, Y. & Kaji, H. Molecular design realizing very fast reverse intersystem crossing in purely organic emitter. ChemRxiv, DOI:10.26434/chemrxiv.9745289 (2019).
19. Allan, D. et al. A novel dual air-bearing fixed-χ diffractometer for small-molecule single-crystal X-ray diffraction on beamline I19 at diamond light source. *Crystals* **7**, 336 (2017).
20. Bailey, S. The CCP4 suite-programs for protein crystallography. *Acta Crystallogr. D* **50,** 760–763 (1994).

21. Evans, P. Scaling and assessment of data quality. *Acta Crystallogr. D* **62,** 72–82 (2006).
22. Winter, G. xia2: an expert system for macromolecular crystallography data reduction. *J. Appl. Cryst.* **43,** 186–190 (2010).
23. Farrugia, L. J. WinGX and ORTEP for Windows: an update. *J. Appl. Crystallogr* **45,** 849–854 (2012).
24. Evans, P. R. & Murshudov, G. N. How good are my data and what is the resolution? *Acta Crystallogr D* **69,** 1204–1214 (2013).
25. Stenkamp, R. E. Identifying G protein-coupled receptor dimers from crystal packings. *Acta Crystallogr. D* **74**, 655–670 (2018).
26. Sheldrick, G. M. SHELXT-integrated space-group and crystal-structure determination. *Acta Crystallogr*. *A* **71,** 3–8 (2015).
27. Sheldrick, G. M. Crystal structure refinement with SHELXL. *Acta Crystallogr. Section C* **71**, 3–8 (2015).